Solid Fuels that Form HOH Catalyst

R. Mills[1], J. Lotoski, W. Good, J. He

BlackLight Power, Inc., 493 Old Trenton Road, Cranbury, NJ 08512, USA

Abstract: Atomic hydrogen is predicted to form fractional Rydberg energy states $H(1/p)$ called "hydrino atoms" wherein $n = \frac{1}{2}, \frac{1}{3}, \frac{1}{4}, ..., \frac{1}{p}$ ($p \leq 137$ is an integer) replaces the well-known parameter $n = \text{integer}$ in the Rydberg equation for hydrogen excited states. The transition of H to a stable hydrino state $H\left[\dfrac{a_H}{p = m+1}\right]$ having a binding energy of $p^2 \cdot 13.6 \ eV$ occurs by a nonradiative resonance energy transfer of $m \cdot 27.2 \ eV$ (m is an integer) to a matched energy acceptor such as nascent H_2O that has a potential energy of 81.6 eV ($m = 3$). The nascent H_2O molecule formed by an oxidation reaction of OH^- at a hydrogen anode is predicted to serve as a catalyst to form $H(1/4)$ with an energy release of 204 eV compared to the 1.48 eV required to produce H from electrolysis of H_2O. CIHT cells, each comprising a LiOH-LiBr eutectic mixture as the electrolyte exploit hydrino formation as a half-cell reaction to serve as a new electrical energy source. Net electrical production over the electrolysis input and hydrogen supplied to the anode was measured using an Arbin BT 2000. The electrical energies were continuously output over long-duration, measured on different systems, configurations, and modes of operation and were typically multiples of the electrical input that in most cases exceed the input by a factor of about 2 at about 10 mW/cm^2 anode area. The power density was increased by a factor of over 10 by running a corresponding high current. The thermal energy balance of solid fuels that form the HOH catalyst by a reaction akin to those of CIHT cells were measured using both a water flow calorimeter and a Setaram DSC 131 differential scanning calorimeter (DSC). The DSC results confirmed water flow calorimetric (WFC) results and the former were further independently replicated at Setaram Instrumentation based in France. The thermal energy balance for solid fuels such as $Co(OH)_2$ + $CuBr_2$ and $Cu(OH)_2$ + $CuBr_2$ were up to 60 times the maximum theoretical for both types of calorimeters with supportive XRD of the

---

[1] Corresponding author: 609-490-1090 (phone); 609-490-1066 (fax); rmills@blacklightpower.com

WFC products. DSC performed on FeOOH and $Cu(OH)_2$ + $FeBr_2$ in gold crucibles at Perkin Elmer showed up to four times the maximum theoretical energy. DSC and XRD were independently performed on the starting materials. The MAS ^1H NMR showed a predicted upfield matrix shift of a KOH-KCl hydrino getter when exposed to the gas from a reacting $Cu(OH)_2$ + $CuBr_2$ solid fuel in a sealed cell. A Raman peak starting at 1950 cm^{-1} matched the free space rotational energy of $H_2(1/4)$ (0.2414 eV). The solid fuels scaled linearly to over 5 kW and confirm the energetic reaction of hydrinos and may serve as a thermally reversible system to continuously generate power for commercial uses.

Key Words: new energy source, HOH catalysis, hydrinos, solid fuels

1. Introduction

Classical physical laws applied to atomic systems [1-9] predict that atomic hydrogen may undergo a catalytic reaction with certain species, including itself, that can accept energy in integer multiples of the potential energy of atomic hydrogen, $m \cdot 27.2$ eV, wherein m is an integer. The predicted reaction involves a resonant, nonradiative energy transfer from otherwise stable atomic hydrogen to the catalyst capable of accepting the energy. The product is H(1/p), fractional Rydberg states of atomic hydrogen called "hydrino atoms," wherein $n = 1/2, 1/3, 1/4,\ldots, 1/p$ ($p \leq 137$ is an integer) replaces the well-known parameter n = integer in the Rydberg equation for hydrogen excited states. Each hydrino state also comprises an electron, a proton, and a photon, but the field contribution from the photon increases the binding rather than decreasing it corresponding to energy desorption rather than absorption. A molecule that accepts $m \cdot 27.2 \ eV$ from atomic H with a decrease in the magnitude of the potential energy of the molecule by the same energy may serve as a catalyst. The potential energy of H_2O is 81.6 eV [1]; so, the nascent H_2O molecule (not hydrogen bonded in solid, liquid, or gaseous state) may serve as a catalyst. Based on the 10% energy change in the heat of vaporization in going from ice at 0°C to water at 100°C, the average number of H bonds per water molecule in boiling water is 3.6 [1]; thus, H_2O must be formed chemically as isolated molecules with suitable activation energy in order to serve as a catalyst to form hydrinos. The catalysis reaction $(m = 3)$ regarding the potential energy of nascent H_2O is

$$81.6 \ eV + H_2O + H\left[a_H\right] \rightarrow 2H^+_{fast} + O^- + e^- + H*\left[\frac{a_H}{4}\right] + 81.6 \ eV \tag{1}$$

$$H*\left[\frac{a_H}{4}\right] \rightarrow H\left[\frac{a_H}{4}\right] + 122.4 \ eV \tag{2}$$

$$2H^+_{fast} + O^- + e^- \rightarrow H_2O + 81.6 \ eV \tag{3}$$
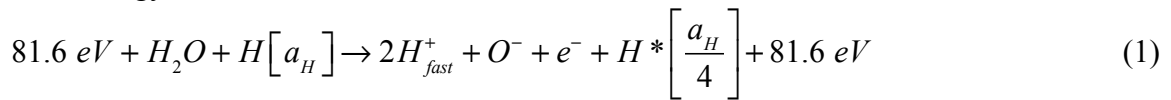
And, the overall reaction is

$$H\left[a_H\right] \rightarrow H\left[\frac{a_H}{4}\right] + 81.6 \ eV + 122.4 \ eV \tag{4}$$

The CIHT electrical energies were continuously output over long-duration, measured on different systems, configurations, and modes of operation and were typically multiples of the electrical input that in recent higher-power-density cases exceed the input by a factor of about 2 at about 10 mW/cm^2 anode area. The power density was further increased by a factor of over 10 while maintaining gain by running a corresponding high current.

Thermal energy may also be produced from the catalysis of H to H(1/4) wherein nascent H_2O serves as the catalyst, and a chemical reaction is the source of atomic hydrogen and catalyst. The H that reacts to form hydrinos may be nascent H formed by reaction of one or more

reactants wherein at least one comprises a source of hydrogen such as the reaction of a hydroxide and an oxide. The reaction may also form H_2O catalyst. The oxide and hydroxide may comprise the same compound. For example, an oxyhydroxide such as FeOOH could dehydrate to provide H_2O catalyst and also provide nascent H for a hydrino reaction during dehydration:

$$4FeOOH \rightarrow H_2O + Fe_2O_3 + 2FeO + O_2 + 2H(1/4) \qquad (5)$$

wherein nascent H formed during the reaction reacts to hydrino. Other exemplary reactions are those of a hydroxide and an oxyhydroxide or an oxide such as NaOH + FeOOH or Fe_2O_3 to form an alkali metal oxide such as $NaFeO_2 + H_2O$ wherein nascent H formed during the reaction may form hydrino wherein H_2O serves as the catalyst. Hydroxide ion is both reduced and oxidized in forming H_2O and oxide ion. Oxide ion may react with H_2O to form OH^-. It was reported previously [10,11] that excess heats from solid fuels reactions were measured using water-flow calorimetry and these results have been independently confirmed by differential scanning calorimetry (DSC) runs at testing laboratories. For example, using their commercial DSC 131 Evo instrument on FeOOH serving as a solid fuel to provide H and H_2O catalyst, Setaram Instrumentation based in France measured three times the maximum theoretical heat of forming H_2O and iron oxides. These products were confirmed by XRD using a Bruker D4 diffractometer.

The same pathway may be obtained with a hydroxide-halide exchange reaction such as the following

$$2M(OH)_2 + 2M'X_2 \rightarrow H_2O + 2MX_2 + 2M'O + 1/2O_2 + 2H(1/4) \qquad (6)$$

wherein exemplary M and M' metals are alkaline earth and transition metals, respectively. An acid-base reaction is another approach to H_2O catalyst. Thus, the thermal chemical reaction is similar to the electrochemical reaction to form hydrinos. The thermal balance of solid fuels was measured using a water flow calorimeter as reported previously [12]. Some of these reactions gave a large thermal burst corresponding to rapid exothermic kinetics developing powers well in excess of 200 W in a 43 cm^3 volume reactor. The predicted molecular hydrino $H_2(1/4)$ was identified as a product of CIHT cells and solid fuels by MAS ^1H NMR, ToF-SIMS, ESI-ToFMS, electron-beam excitation emission spectroscopy, Raman spectroscopy, photoluminescence emission spectroscopy, FTIR, and XPS [10,11].

In the present work, solid fuels $Co(OH)_2$ + $CuBr_2$ and $Cu(OH)_2$ + $CuBr_2$ were run in both a water flow calorimeter (WFC) and a differential scanning calorimeter (DSC), and the results compared. Moreover, the DSC results on $Cu(OH)_2$ + $CuBr_2$ were further independently replicated at Setaram, and DSC was performed on FeOOH and $Cu(OH)_2$ + $FeBr_2$ in gold crucibles at Perkin Elmer's Field Application Laboratory. The maximum theoretical energy for the measured thermal energy balance for a solid fuel such as was confirmed by XRD of the WFC products. DSC and XRD were independently performed on the starting materials.

2. Experimental

2.1. Water-flow, batch calorimetry

The energy balance of the solid fuel reaction mixtures were obtained using cylindrical stainless steel reactors of approximately 43 cm^3 volume (1" inside diameter (ID), 5" length, and 0.060" wall thickness having an internal thermocouple well) and a water flow calorimeter comprising a vacuum chamber containing each cell and an external water coolant coil that collected 99+% of the energy released in the cell to achieve an error $< \pm 1\%$. The water-flow calorimeter was scaled-up using the previous design to accommodate a 20-fold increase in power measurement. The method of measure was the same as that of the smaller-scale with appropriate corresponding time intervals. Both the cells and water-flow calorimeter were described previously [13,14].

2.2. Differential scanning calorimeter (DSC) measurements

A Setaram DSC 131 was used to measure the thermal energy balance of solid fuels. Prior to sample measurements, the DSC (Setaram DSC131) was calibrated for enthalpy and temperature by using pure indium that served as a standard (T_m onset of 156.6 °C, ΔH of 28.71 J/g) for the melting point and enthalpy of melting. Hermetically sealed 30 mm^3 Incoloy crucibles (Part#: S60/58186, Setaram), designed to resist to any possible high-pressure gas produced by the decomposition of the sample were used for all calibration and sample measurements. Dry nitrogen was flowed at a rate of 30 ml/min as the purge gas. Additionally, two samples were loaded into gold pressure pans with gold seals (Product Number B0182902) under argon atmosphere at the Blacklight Power and returned to the Perkin Elmer Applications Laboratory (PEFAL) for DSC analysis. The two samples were analyzed using the Perkin Elmer DSC 8000. Samples (approximately 10–15 mg) were loaded into the crucible and sealed while in a dry box having an argon atmosphere. The reference crucible was empty. For all tests, the samples were initially equilibrated at 30 °C for 20 min, heated from 30 °C to 350 °C (450 °C PEFAL) at the rate of 10 °C/min, cooled from 350 °C to 30 °C at 10 °C/min, and finally equilibrated at 30 °C for 20 min.

2.3. Quantitative X-ray diffraction (XRD)

XRD was performed on the starting materials and the reaction products using hermetically sealed sample holders (Bruker Model #A100B37) loaded in a glove box under argon, wax sealed, and

analyzed with a Siemens D5000 diffractometer using Cu radiation at 40kV/40mA over the range 10°–80° with a step size of 0.02° and a counting time of 143 seconds per step. Once the patterns had been obtained, the phases were identified with the aid of the ICDD database and quantified by a Rietveld refinement.

2.4. MAS ^1H NMR

^1H MAS NMR was performed on solid samples using a 270 MHz instrument with a spin speed of 4.5 kHz. Chemical shifts were referenced to external TMS. Inorganic compound getter KCl-KOH mixture was placed in the sealed container of closed cells wherein hydrinos generated during operation were trapped in the matrix of the compound that thereby served as a molecular hydrino getter. Starting materials not exposed to a hydrino source served as controls.

2.5. Raman spectroscopy

Raman spectroscopy was performed on MoCu foils that each served as a getter or collector of the hydrino gas from the reaction of $Cu(OH)_2 + CuBr_2$ maintained at 350 °C in a sealed stainless steel reactor. The instrument was a Thermo Scientific DXR SmartRaman spectrometer having a 780 nm diode laser. The resolution, depending on the instrument focal length, wavelength range, and grating, was typically 1–5 cm^{-1}.

3. Results and discussion

The energy recovery for water-flow batch calorimetry was determined by integrating the total output power P_T over time. The power was given by

$$P_T = \dot{m}C_p\Delta T \tag{7}$$

where $\dot{m}$ was the mass flow rate, C_p was the specific heat of water, and ΔT was the absolute change in temperature between the inlet and outlet. The reaction was initiated by applying precision power to external heaters. Specifically, 200 W of power was supplied to the heater. During this heating period, the reagents reached a hydrino reaction threshold temperature wherein the onset of reaction was typically confirmed by a rapid rise in cell temperature. Once the cell temperature reached about 350 °C the input power was set to zero. To increase the rate of heat transfer to the coolant, the chamber was re-pressurized with 1000 Torr of helium, and the maximum change in water temperature (outlet minus inlet) was approximately 1.2 °C. The

assembly was allowed to fully reach equilibrium over a 24-hour period as confirmed by the observation of full equilibrium in the flow thermistors.

In each test, the energy input and energy output were calculated by integration of the corresponding power. The thermal energy in the coolant flow in each time increment was calculated using Eq. (7) by multiplying volume flow rate of water by the water density at 19 °C (0.998 kg/liter), the specific heat of water (4.181 kJ/kg °C), the corrected temperature difference, and the time interval. Values were summed over the entire experiment to obtain the total energy output. The total energy from the cell E_T must equal the energy input E_{in} and any net energy E_{net}. Thus, the net energy was given by

$$E_{net} = E_T - E_{in}. \tag{8}$$

From the energy balance, any excess heat E_{ex} was determined relative to the maximum theoretical E_{mt} by

$$E_{ex} = E_{net} - E_{mt}. \tag{9}$$

The calibration test results demonstrated a heat coupling of better than 98% of the resistive input to the output coolant, and zero excess heat controls demonstrated that with the calibration correction applied, the calorimeter was accurate to within less than 1% error. The results are given in Table 1 where T_{max} is the maximum cell temperature, and the energy gain is given by $\dfrac{E_{net}}{-E_{mt}}$. All theoretical energies are negative when exothermic. Positive output values represent more output than input energy. Typical energy balances measured by absolute water-flow calorimetry were 3.3 to more than 60 times energy gain relative to the maximum theoretical based on the most exothermic reactions possible, and power levels in excess of 4.5 Wcm^{-3} were reproducibly achieved. The reaction scaled linearly to 361.5 kJ that developed conservatively over 2 kW and a system-response-corrected power of over 5 kW [13]. Moreover, the chemistries are enabling of thermal regeneration of the products back to reactants as a competitive fuel cycle for thermal power production with H_2O as the source of hydrogen fuel to form hydrinos replacing traditional fossil fuels.

Table 1 – The solid fuel reactants, maximum temperature of the run T, experimental net energy E_{net}, calculated theoretical maximum energy E_{mt} for conventional chemistry [18–20], and energy gain of hydrino catalyst systems.

Cell No.	Chemicals	T_{max} °C	E_{net} kJ	E_{mt} kJ	Energy Gain
141	25.0g FeOOH	501	6.0	-1.4	4.3
172	25.0g FeOOH (AD-1)	577	8.8	-1.4	6.3
181[1]	25.0g FeOOH (AD-1)	563	7.4	-1.4	5.3
465	9.8g Cu(OH)$_2$ + 21.6g FeBr$_2$ + 1 atm Ar	565	13.9	-1.6	8.7
466	9.8g Cu(OH)$_2$ + 21.9g NiBr$_2$ + 1 atm Ar	591	17.3	-0.9	19.2
467[2]	9.8g Cu(OH)$_2$ + 21.9g CoBr$_2$ + 1 atm Ar	576	12.0	-1.1	10.9
468	9.8g Cu(OH)$_2$ + 13.0g NiCl$_2$ + 1 atm Ar	552	8.7	0.6	inf
469	9.8g Cu(OH)$_2$ + 21.5g MnBr$_2$ + 1 atm Ar	603	14.2	9.8	inf
470[3]	9.8g Cu(OH)$_2$ + 27.9g SnBr$_2$ + 1atm Ar	598	16.4	-1.5	10.9
471[4]	9.8g Cu(OH)$_2$ + 19.0g SnCl$_2$ + 1 atm Ar	623	20.2	-1.2	16.8
475	9.8g Cu(OH)$_2$ + 37.3.0g SnI$_2$ + 1atm Ar	507	13.4	-4.1	3.3
479[5]	14.6g Cu(OH)$_2$ + 15.0g InCl$_3$ +1atm Ar (repeat)	568	16.4	-0.6	27.3
510	9.3g Co(OH)$_2$ + 13.5g CuCl$_2$ + 1atm Ar	554	7.8	-0.3	26.0
512[6]	9.3g Co(OH)$_2$ + 23.3g CuBr$_2$ + 1atm Ar	596	15.0	1.1	inf
513	9.3g Ni(OH)$_2$ + 23.3g CuBr$_2$ +1atm Ar	626	17.3	0.9	inf
515	9.8g Cu(OH)$_2$ + 22.3g CuBr$_2$ + 1 atm Ar	630	18.5	0	inf
530[7]	9.3g Co(OH)$_2$ + 23.3g CuBr$_2$ + 1atm Ar	615	15.5	-0.2	77.5
531	9.3g Ni(OH)$_2$ + 23.3g CuBr$_2$ +1atm Ar	599	13.9	-0.9	15.4
532[8]	9.8g Cu(OH)$_2$ + 23.3g CuBr$_2$ + 1 atm Ar	672	21.6	-1.3	16.6
552[9]	9.8g Cu(OH)$_2$ + 21.6g FeBr$_2$ + 1atm Ar	580	13.1	-1.6	8.2
594	20.0g Cu(OH)$_2$ + 26.8g CuCl$_2$ + 1 atm Ar (2x)	462	14.3	-2.6	5.5
703	9.3g Co(OH)2 + 23.3g CuBr2 + 2.0g AC + 1 atm Ar	589	12.4	-0.2	62.0
755	9.3g Co(OH)2 + 23.3g CuBr2 + 100 psi H2	350	9.3	-1.9	4.9

[1] Thermal burst observed 150–170 °C
[2] Thermal burst observed 81–241°C
[3] Thermal burst observed 71–152 °C
[4] Thermal burst observed 54–174 °C
[5] Thermal burst observed 87–169 °C
[6] Thermal burst observed 85–201 °C
[7] Thermal burst observed 78–189 °C
[8] Thermal burst observed 360–520 °C
[9] Thermal burst observed 79–187 °C

Representative WFC results for solid fuel Cu(OH)$_2$ + CuBr$_2$ and control runs of the separate reaction mixture components are given in Table 2, the corresponding calorimetric traces are given in Fig. 1–5, and the theoretical energies for conventional reactions are given in Table 3

with a calculation of the excess thermal energy over the maximum theoretical by those conventional reactions. The confirmation of the starting materials and reaction products to match the calculations is shown by the XRD data given in Fig. 6a–c. The WFC results for the twenty-fold scale-up $Cu(OH)_2$ + $CuBr_2$ run are given in Table 4 with the theoretical energies for conventional reactions and a calculation of the excess thermal energy over the maximum theoretical by those conventional reactions. The corresponding calorimetric traces are given in Fig. 7.

Table 2. WFC results of $CuBr_2$ + $Cu(OH)_2$, and control experiments.

Sample ID	Chemicals	Burst, ºC	Tmax ºC	E_{in} kJ	E_{net} kJ *	$E_{Theoretical}$ kJ	Energy Gain, DE / $E_{Theoretical}$
070312JH WF2-718	23.3g $CuBr_2$ (not dry) + 9.8g $Cu(OH)_2$ (not dry) + 1 atm Ar (load in air)	68–151	354	109.5	10.7	-1.3	8.2
070312JH WF5-720	23.3g $CuBr_2$ (not dry)+ 9.8g $Cu(OH)_2$ (not dry) + 1 atm Ar (load in air)	71–135	360	121.0	8.2	-1.3	6.3
071612JH WF1-724	23.3g $CuBr_2$ (not dry) + 9.8g $Cu(OH)_2$ (not dry) + 1 atm Ar (load in air)	none	324	95.8	8.1	-1.3	6.2
111612JH WF-SU-830	23.3g $CuBr_2$ (not dry) + 9.8g $Cu(OH)_2$ (not dry) + 1 atm Ar (load in air)	98.5–143 [1]	275	1903.6	361.5	-29.57	12.2
071212JH WF1-721	23.3g $CuBr_2$ (not dry) + 1 atm Ar (load in air)	none	288	95.8	-2.0	1.3	endo
071212JH WF4-723	9.8g $Cu(OH)_2$ (not dry) + 1 atm Ar (load in air)	none	256	97.0	-1.6	0.7	endo

[1] Thermal burst observed 98.5–142.6 ºC

Fig. 1 – WFC traces of the power input, thermal output, cell temperature, and cell pressure for 070312JHWF2-718.
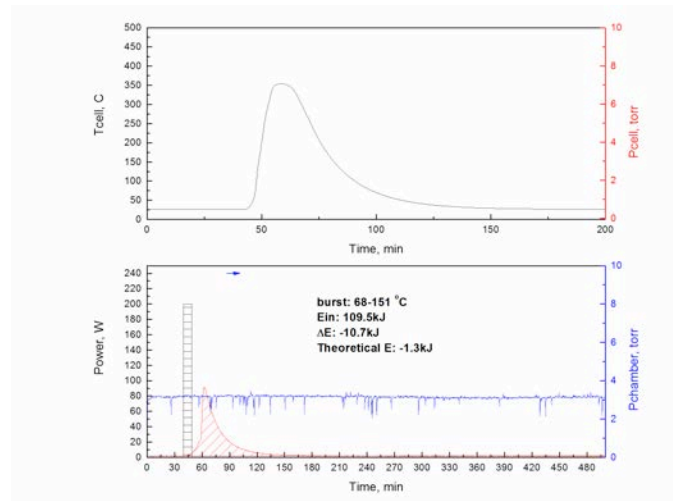
Fig. 2 – WFC traces of the power input, thermal output, cell temperature, and cell pressure for 070312JHWF5-720.
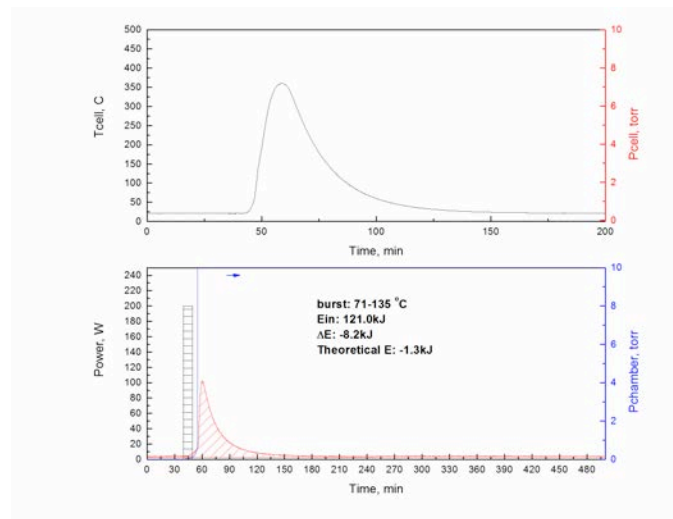
Fig. 3 – WFC traces of the power input, thermal output, cell temperature, and cell pressure for 071612JHWF1-724.
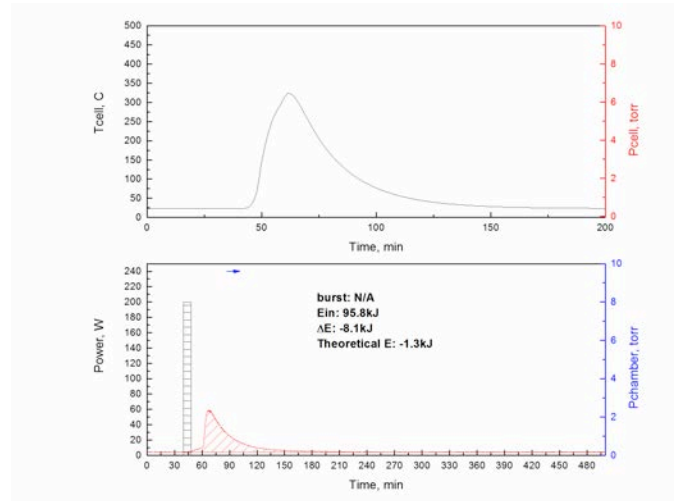
Fig. 4 – WFC traces of the power input, thermal output, cell temperature, and cell pressure for 071212JHWF1-721.
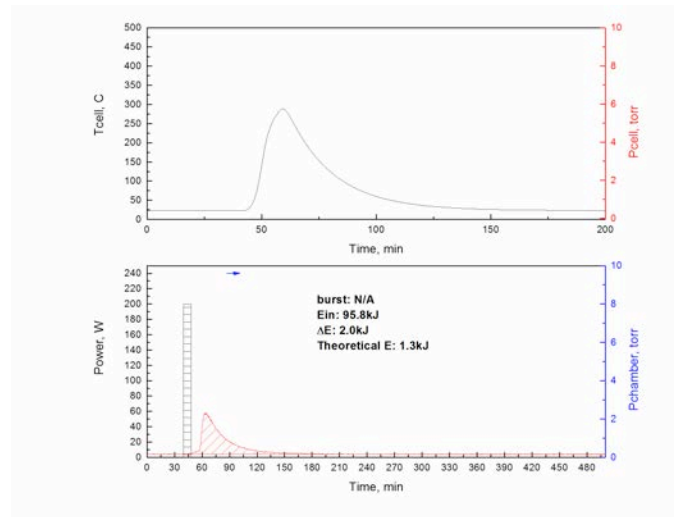
Fig. 5 – WFC traces of the power input, thermal output, cell temperature, and cell pressure for 071212JHWF4-723.
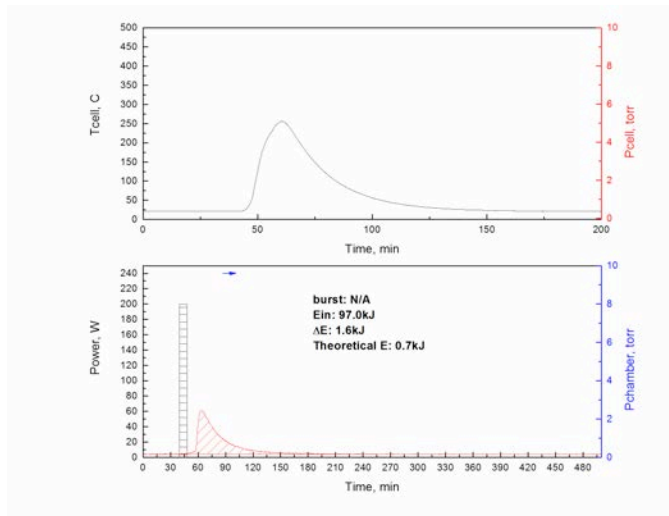
Table 3 – Theoretical calculations of the heat generated by conventional reactions of each reactant and the mixture of $Cu(OH)_2$ + $CuBr_2$.

Cell: 071212JHWF2-721, $CuBr_2$ + Ar					
Reactant $\quad$ $CuBr_2$				E_{net}, kJ	Excess energy, kJ
Quantity, g $\quad$ 23.30				-2.00	-0.71
Quantity, mol 0.1043					
Assumed Reaction	Energy, kJ/reaction	$CuBr_2$ consumed, mol	$CuBr_2$ left, mol	Energy out, kJ	Theo Energy, kJ
$CuBr_2 = CuBr + 1/2\ Br_2$	37.20	0.1043	0.0000	1.29	1.29

Cell: 071212JHWF4-723, $Cu(OH)_2$ + Ar					
Reactant $\quad$ $Cu(OH)_2$				E_{net}, kJ	Excess energy, kJ
Quantity, g $\quad$ 9.80				-1.60	-0.91
Quantity, mol $\quad$ 0.1005					
Assumed Reaction	Energy, kJ/reaction	$Cu(OH)_2$ consumed, mol	$Cu(OH)_2$ left, mol	Energy out, kJ	Theo Energy, kJ
$Cu(OH)_2 = CuO + H_2O$	6.90	0.1005	0.0000	0.69	0.69

Cell: 070312JHWF2-718, $Cu(OH)_2$ + $CuBr_2$ + Ar									
Reactant	$Cu(OH)_2$	$CuBr_2$					E_{net}, kJ	Excess energy, kJ	Gain
Quantity, g	9.80	23.30					10.70	9.38	7.10
Quantity, mol	0.1005	0.1043							
Assumed Reaction	Energy, kJ/reaction	$Cu(OH)_2$ consumed, mol	$CuBr_2$ consumed, mol	$Cu(OH)_2$ left, mol	$CuBr_2$ left, mol	Energy out, kJ	Theo Energy, kJ		
$Cu(OH)_2 + CuBr_2 = CuBr_2 + Cu(OH)_2$	0.00	0.1005	0.1005	0.0000	0.0000	0.00	0.00		
$Cu(OH)_2 + CuBr_2 = CuBr_2.H_2O + CuO$	-13.10	0.1005	0.1005				-1.32		
$CuBr_2 = CuBr + 1/2\ Br_2$	37.20								
$Cu(OH)_2 = CuO + H_2O$	6.90								

13

Fig. 6 – XRD phase identification for products from: (a) sample 070312JHWF2-718, (b) sample $CuBr_2$ (starting chemical), and (c) sample $Cu(OH)_2$ (starting chemical).
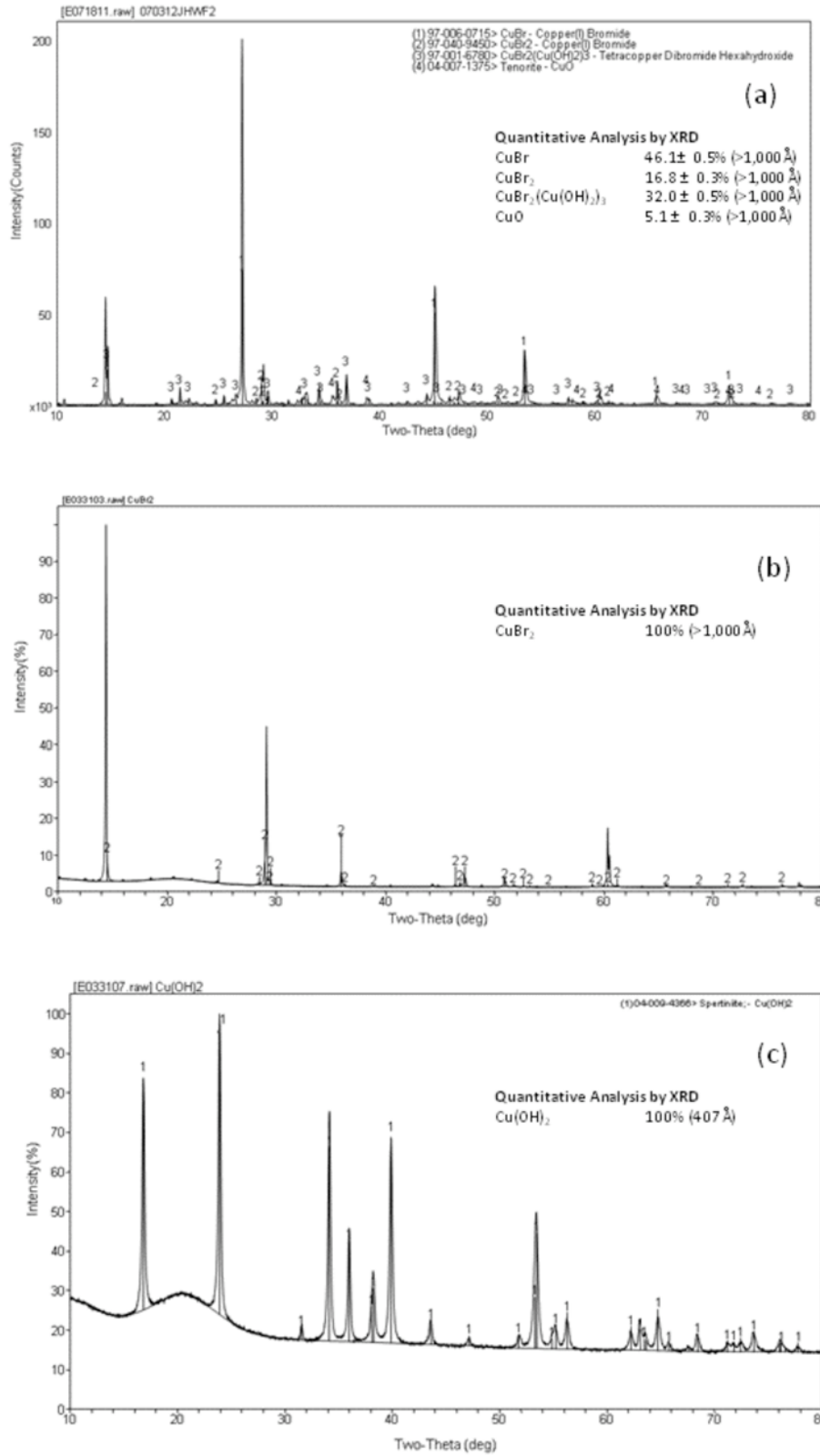
Table 4 – Theoretical calculations of the heat generated by conventional reactions of each reactant and the mixture of $Cu(OH)_2 + CuBr_2$ in the scale-up run.

Cell: 111612JHWF-SU-830, $Cu(OH)_2 + CuBr_2 + Ar$								
Reactant	$Cu(OH)_2$	$CuBr_2$				E_{net}, kJ	Excess energy, kJ	Gain
Quantity, g	220.60	504.10				361.50	331.93	12.22
Quantity, mol	2.2626	2.2575						
Assumed Reaction	Energy, kJ/reaction	$Cu(OH)_2$ consumed, mol	$CuBr_2$ consumed, mol	$Cu(OH)_2$ left, mol	$CuBr_2$ left, mol	Energy out, kJ	Theo Energy, kJ
$Cu(OH)_2 + CuBr_2 = CuBr_2 + Cu(OH)_2$							
$Cu(OH)_2 + CuBr_2 = CuBr_2.H_2O + CuO$	-13.10	2.2575	2.2575	0.0051	0.0000		-29.57

Fig. 7 – WFC traces of the power input, thermal output, and cell temperature for the scale-up run. The power given by dividing the temperature rise that occurred when the chemicals reacted by the total response time was 2.1 kW. The system-response corrected power was about 5 kW [13].
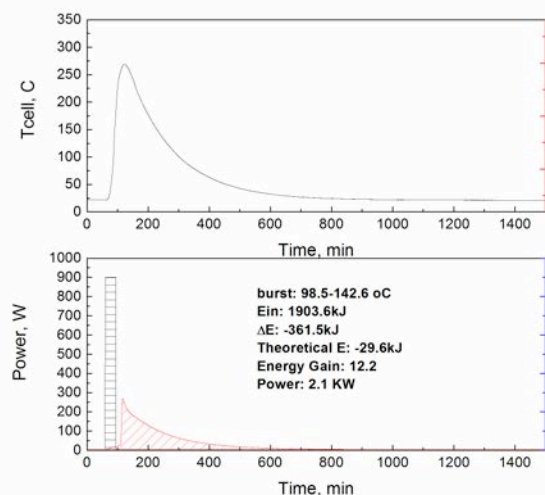
Representative DSC results on solid fuels $Co(OH)_2 + CuBr_2$ and $Cu(OH)_2 + CuBr_2$ are given in Tables 5 and 6, wherein the energy gain over the maximum theoretical energy were over 60 times and 8 times, respectively. $Cu(OH)_2 + CuBr_2$ and controls run of the separate reaction mixture components are also given in Table 5, and the corresponding heating and cooling traces are given in Fig. 8a–f. The Setaram verification data on solid fuel $Cu(OH)_2 + CuBr_2$ is shown in Table 7 and Fig. 9a–b. The WFC and DSC results confirmed by Setaram were reproducible and

in agreement. The Perkin Elmer DSC data on solid fuels FeOOH and $Cu(OH)_2$ + $FeBr_2$ run in inert gold, sealed pans compared to the maximum theoretical energies is shown in Tables 8 and 9, respectively.

Table 5 – Exemplary DSC test results on $Co(OH)_2$ + $CuBr_2$.

Date	Chemical	Heating (J/g)	Cooling (J/g)	Exp. Total (J/g)	Theo Energy (J/g)	Energy Gain
9/26/2012	21.1mg ($Co(OH)_2$ + $CuBr_2$; 1:1)	-266.6	0	-266.6	-4.90	54.41
9/26/2012	21.3mg ($Co(OH)_2$ + $CuBr_2$; 1:1)	-336.9	0	-336.9	-4.90	68.76
9/27/2012	21.9mg ($Co(OH)_2$ + $CuBr_2$; 1:1)	-307.7	0	-307.7	-4.90	62.80
9/27/2012	25.4mg ($Co(OH)_2$ + $CuBr_2$; 1:1)	-326.8	0	-326.8	-4.90	66.69

Table 6 – DSC results on $CuBr_2$ + $Cu(OH)_2$ and controls.

Date	Chemical	Heating (J/g)	Cooling (J/g)	Exp. Total (J/g)	Theo Energy (J/g)	Energy Gain
7/19/12	9.8mg $CuBr_2$ + 1 atm Ar*	0	0	0	0	0.00
7/25/2012	7.5mg $Cu(OH)_2$ + 1 atm Ar	368.70	0	368.70	70.80	endo
7/24/2012	3.8mg $Cu(OH)_2$ + 8.6mg $CuBr_2$ + 1 atm Ar	-346.40	0	-346.40	-40.69	8.50
8/7/2012	3.2mg $Cu(OH)_2$ + 7.6mg $CuBr_2$ + 1 atm Ar (pre-mix)	-331.34	0	-331.34	-41.28	8.03

* maximum temperature was set at 350 $^{\circ}$C.

Fig. 8 – (a) CuBr$_2$, DSC heating trace; (b) DSC CuBr$_2$ cooling trace; (c) DSC Cu(OH)$_2$, heating trace; (d) DSC Cu(OH)$_2$, cooling trace; (e) DSC CuBr2 + Cu(OH)$_2$, heating trace, with maximum temperature at 350 ºC; and (f) DSC CuBr$_2$ + Cu(OH)$_2$, cooling trace, with maximum temperature at 350 ºC.
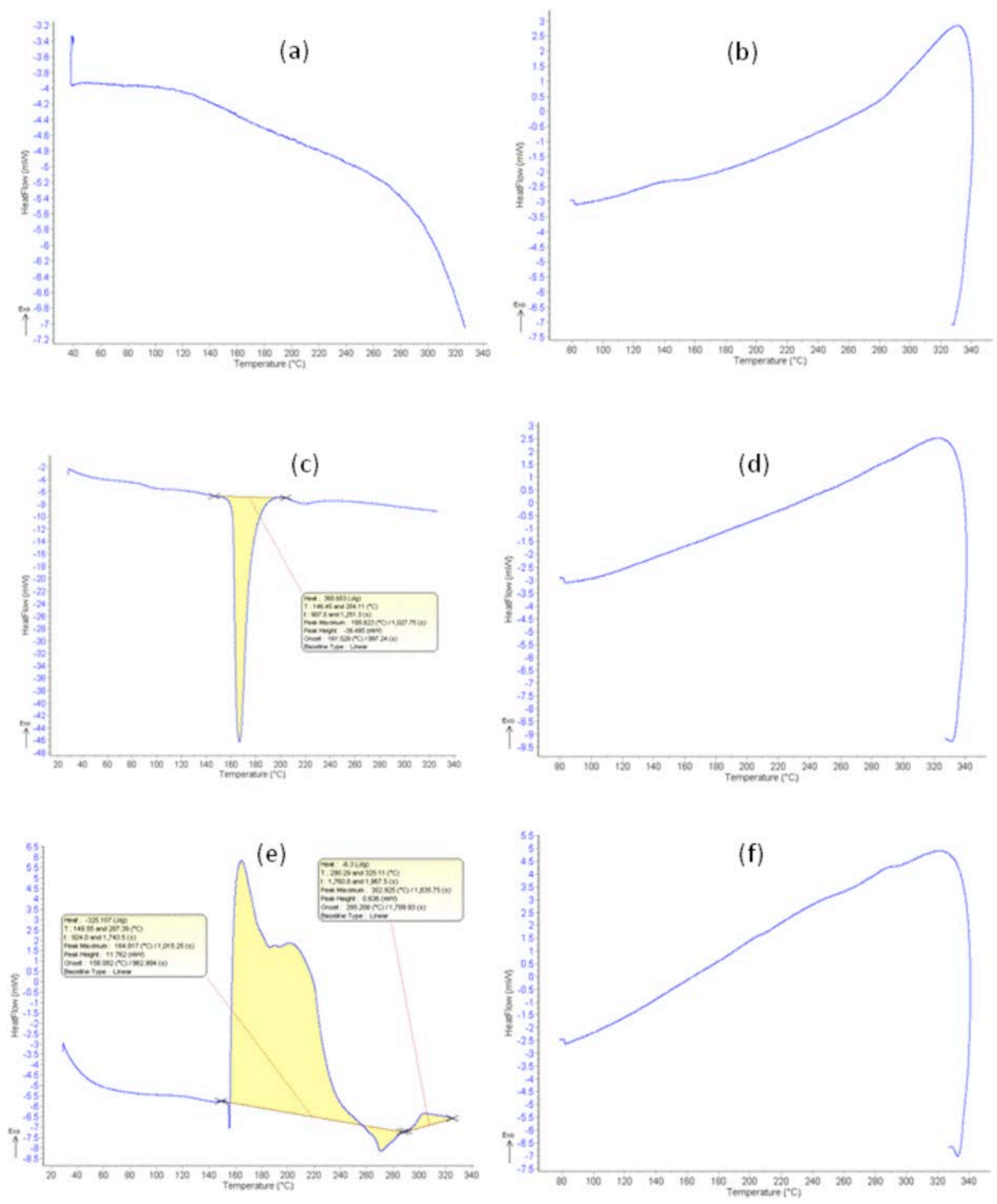
Table 7 – Confirming DSC results performed by Setaram, Caluire, France on $Cu(OH)_2$ and $CuBr_2$.

Sample	Exotherm	
	Top of Peak	Heat
092012JL1M1 Heating	167.7 ºC–223.8 ºC	-323.13 J/g
092012JL1M3 Heating	145.4 ºC–181.6 ºC–220.9 ºC	-430.86 J/g

Fig. 9 – (a) DSC performed on $Cu(OH)_2$ + $CuBr_2$ by Setaram. The theoretical energy was -39.8 J/g based on the limiting reagent such that the DSC exothermic energy of -323.1 J/g corresponded to an energy gain of 8.1 times the maximum theoretical from conventional chemistry; (b) Duplicate DSC performed on $Cu(OH)_2$ + $CuBr_2$ by Setaram. The theoretical energy was -39.8 J/g based on the limiting reagent such that the DSC exothermic energy of -430.9 J/g corresponded to an energy gain of 10.8 times the maximum theoretical from conventional chemistry.
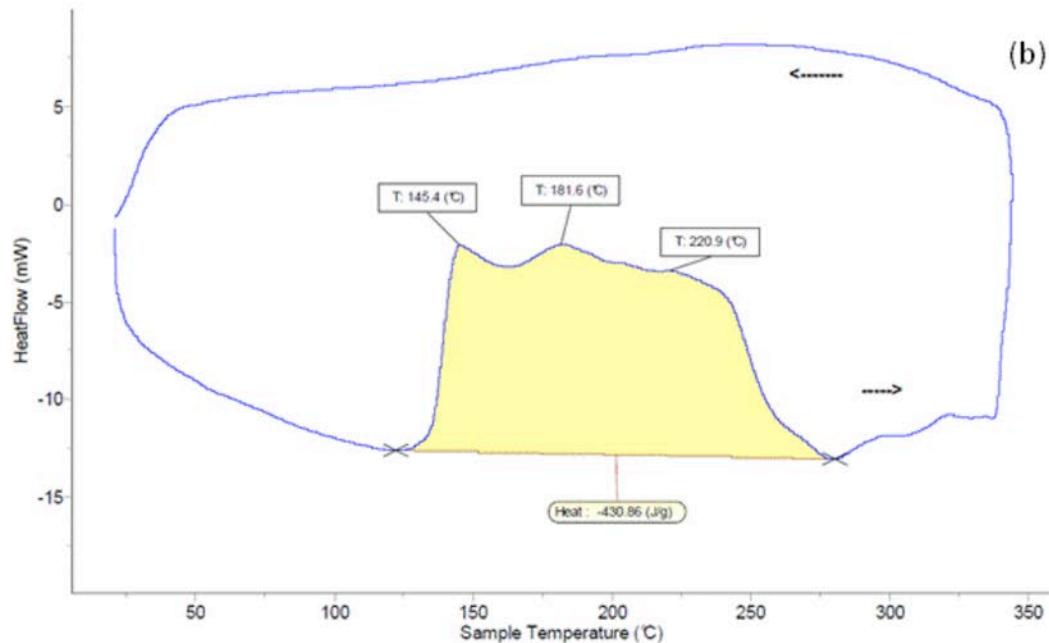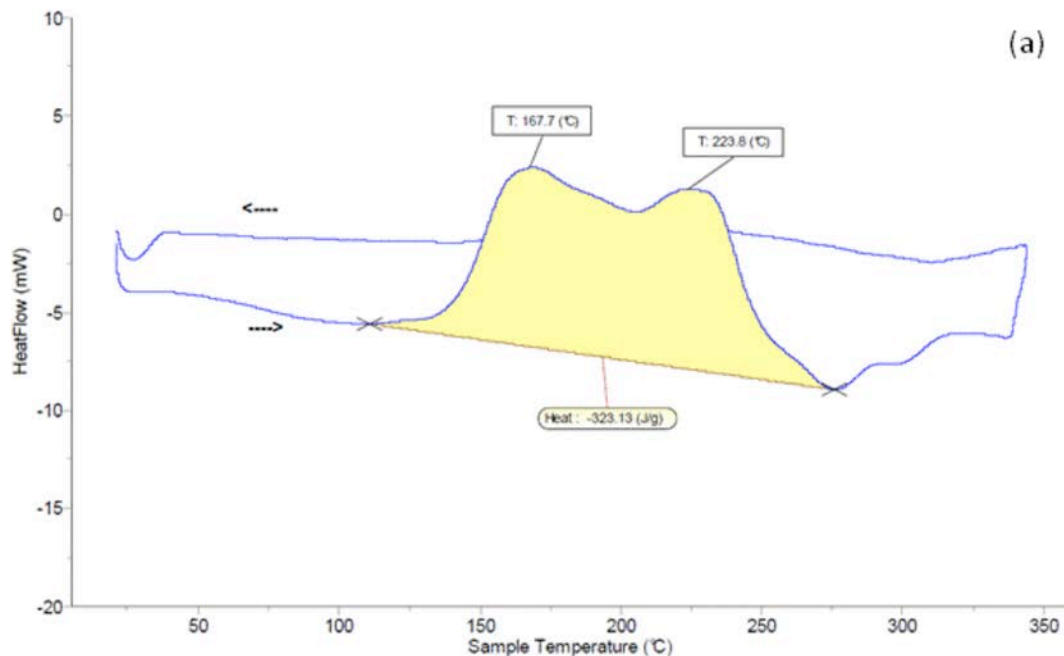
Table 8 – The Perkin Elmer DSC data on solid fuel FeOOH run in an inert gold, sealed pan compared to the maximum theoretical energy.

DSC–Perkin Elmer: 101413JH1 (sample 1), FeOOH + Ar					_E, J/g	Excess energy, kJ	Energy Gain
Reactant	FeOOH						
Quantity, mg	6.30				-158.46	-158.46	3.07
Quantity, mmol	0.0708						
Assumed Reaction		Energy, kJ/reaction	FeOOH consumed, mmol	FeOOH left, mmol		Energy out, kJ	Theo Energy, kJ
$2FeOOH = Fe_2O_3 + H_2O$		-9.20	0.0708	0.0000		-0.33	-51.69

Table 9 – The Perkin Elmer DSC data on solid fuel $Cu(OH)_2$ + $FeBr_2$ run in an inert gold, sealed pan compared to the maximum theoretical energy.

DSC–Perkin Elmer: 101413JH2 (sample 2), $Cu(OH)_2 + FeBr_2$								_E, J/g	Excess energy, kJ	Energy Gain
Reactant	$FeBr_2$	$Cu(OH)_2$								
Quantity, mg	5.70	2.40						-243.79	-180.52	3.85
Quantity, mmol	0.0264	0.0246								
HOF, dH (KJ/mol)	-249.80	-450.00								

Product	$Fe(OH)_2$	$CuBr_2$	Fe_2O_3	$FeBr_2.2H_2O$	CuBr	Cu_2O	FeO	H_2O	HBr(g)
HOF, dH (KJ/mol)	-574.00	-141.80	-822.20	-861.40	-104.60	-168.60	-272.00	-285.80	-36.60

Assumed Reaction I	Energy, kJ/reaction	$FeBr_2$ used, mmol	$Cu(OH)_2$ used, mmol	$Cu(OH)_2$ left, mmol	$FeBr_2$ left, mmol	Energy out, kJ	Theo Energy, kJ
$Cu(OH)_2 + FeBr_2 = Fe(OH)_2 + CuBr_2$	-16.00	0.0246	0.0246	0.0000	0.0018	-0.39	-48.62
$10Cu(OH)_2 + 9FeBr_2 = 2Fe_2O_3 + 5FeBr_2.2H_2O + 8CuBr + Cu_2O + 3/2\ O_2$	-208.20	0.0222	0.0246	0.0000	0.0043	-0.51	-63.27
$3Cu(OH)_2 + 3FeBr_2 = Fe_2O_3 + FeO + 3CuBr + 2H_2O + 2HBr + 1/2\ Br_2$	47.40	0.0246	0.0246			0.39	

The predicted hydrino product $H_2(1/4)$ was identified by MAS ^1H NMR and Raman spectroscopy. MAS NMR of molecular hydrino trapped in a protic matrix represents a means to exploit the unique characteristics of molecular hydrino for its identification via its interaction with the matrix due to the possession of quantum states $H_2\left(1/p\right)$ have states with $\ell = 0,1,2,...,p-1$ that gives rise to a magnetic moment [1] that could cause an upfield matrix shift. The KOH-KCl (1:1) getter showed a shift of the MAS NMR active component of the matrix (KOH) from downfield at +4.4 ppm to upfield at –4.4 ppm after exposure to the atmosphere inside of the sealed cell (Fig. 10a–b). The different ℓ quantum numbers possible for the p = 4 state can give rise to different upfield matrix shifts consistent with observations of multiple such peaks in the region of -4 ppm.

Fig. 10 – (a)^1H MAS NMR spectrum relative to external TMS of the initial KOH-KCl (1:1) getter that shows the known down-field shifted matrix peak at +4.44 ppm; (b) ^1H MAS NMR spectrum relative to external TMS of the KOH-KCl (1:1) getter from sealed $Cu(OH)_2$ + $CuBr_2$ reaction cell showing upfield shifted peak at -4.42 ppm. The symmetrically spaced peaks are spinning side bands.
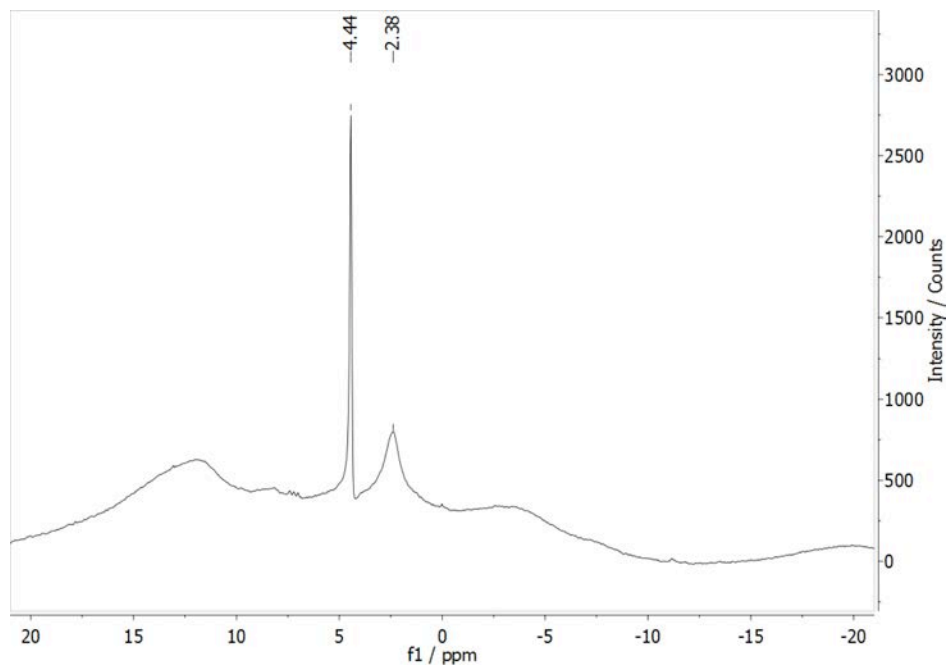
(a)
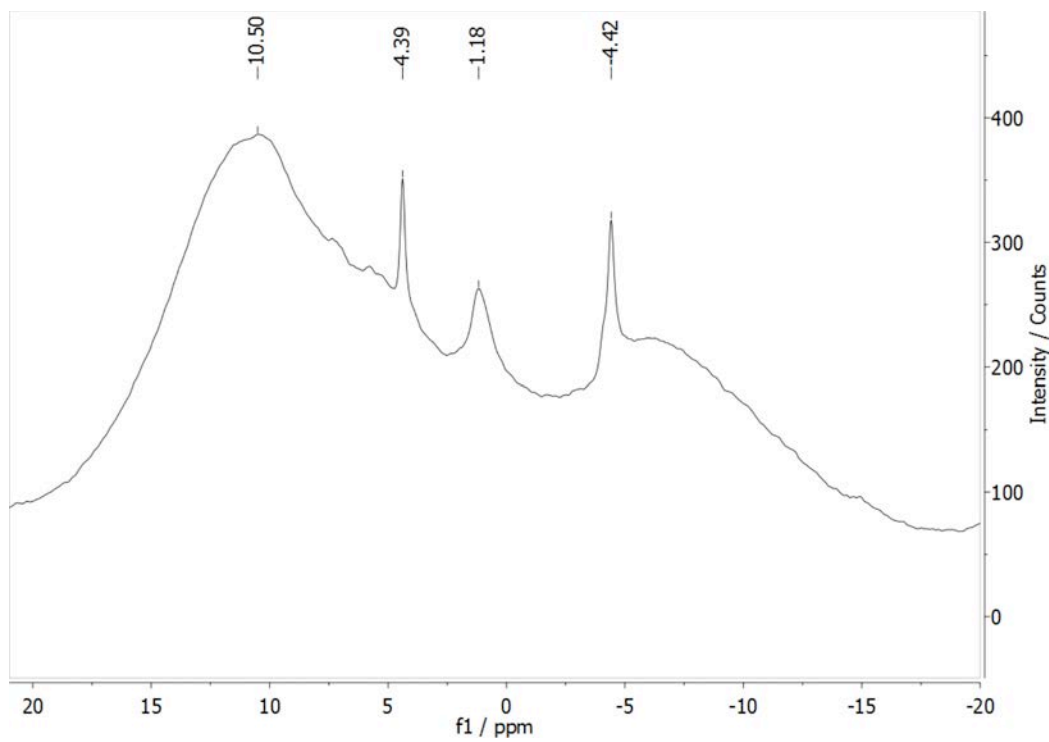
(b)

Using a Thermo Scientific DXR SmartRaman with a 780 nm diode laser in the macro mode, an absorption peak was observed on the product of the $Cu(OH)_2$ + $CuBr_2$ reaction (Fig. 11a) and on a MoCu getter after the production of excess thermal energy (Fig. 11b–d). The peak was not observed in the MoCu virgin alloy (Fig. 11b), and the peak intensity increased with increasing laser intensity. The only possible elements to consider as the source were Mo, Cu, H, and O. Permutations of control compounds did not reproduce the peak. The same peak having a width of 40 cm^{-1} was observed on MoCu permeation anodes of CIHT cells. Since no other element or compound is known that can absorb a single 40 cm^{-1} (0.005 eV) near infrared line at 1.33 eV (the energy of the 780 nm laser minus 2000 cm^{-1}) $H_2(1/4)$ was considered. The absorption peak starting at 1950 cm^{-1} matched the free space rotational energy of $H_2(1/4)$ (0.2414 eV) to four significant figures, and the width of 40 cm^{-1} matches the orbital-nuclear coupling energy splitting [1]. The absorption was assigned to an inverse Raman effect (IRE) [15] peak for the $H_2(1/4)$ rotational energy for the $J' = 1$ to $J'' = 0$ transition [1] as described previously [10,11].

Fig. 11 – The Raman spectra obtained on the product of the $Cu(OH)_2$ + $CuBr_2$ reaction and on a MoCu getter from the solid fuels $Cu(OH)_2$ + $CuBr_2$ using the Thermo Scientific DXR SmartRaman spectrometer and the 780 nm laser showing an inverse Raman effect absorption peak starting at 1950 cm^{-1} that matches the free rotor energy of $H_2(1/4)$ (0.2414 eV) to four significant figures. (a) $Cu(OH)_2$ + $CuBr_2$ reaction product showing the IRE peak at 2000 cm^{-1}. (b) MoCu starting material showing no peak. (c) MoCu getter showing the IRE peak at 1996 cm^{-1}. (d) MoCu getter covered by getter of Fig. 11c showing the IRE peak at 1984 cm^{-1} at a lesser intensity due to being covered.
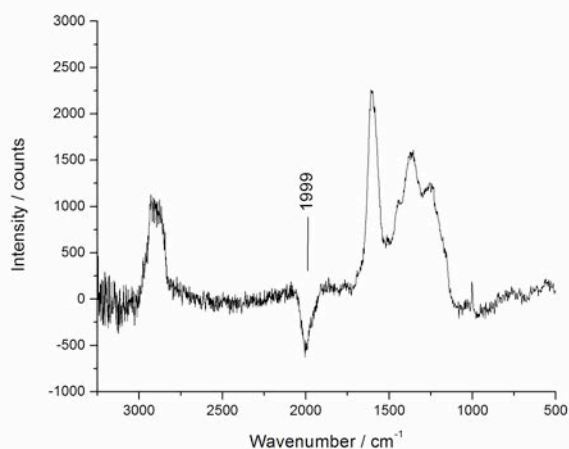
(a)
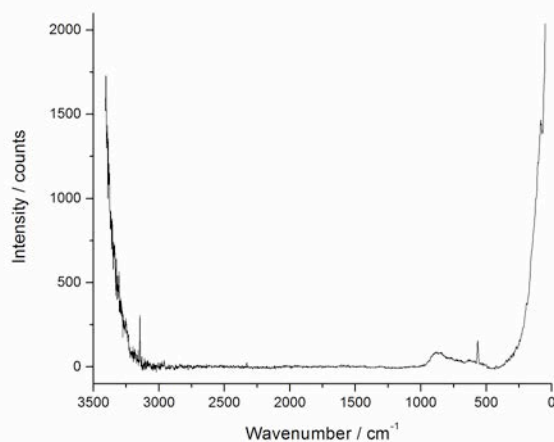
(b)
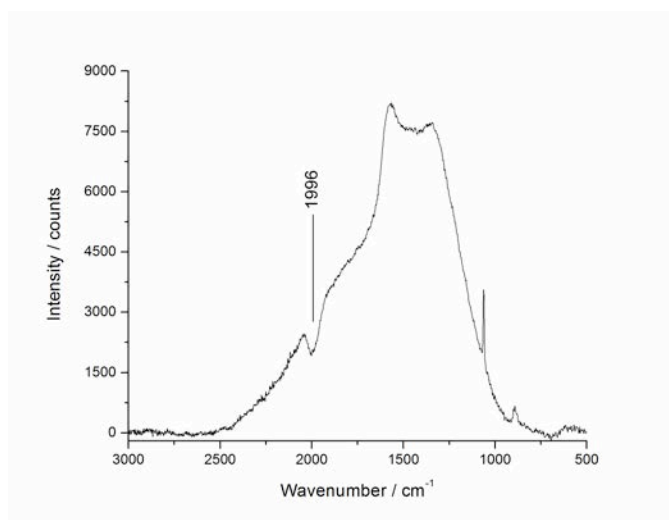
(c)
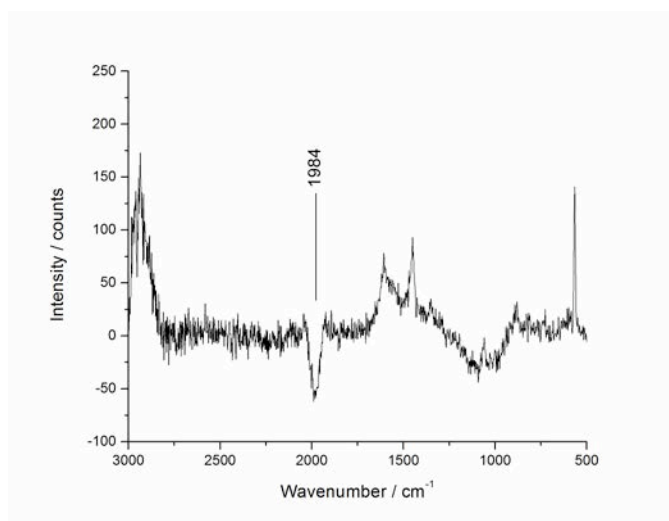
(d)

4. Conclusion

Solid fuels were run in both a water flow calorimeter (WFC) and a differential scanning calorimeter (DSC), and the results matched. Moreover, the DSC results were further independently replicated at Setaram and Perkin Elmer's Field Applications Laboratory. The thermal energy balance for solid fuels such as $Co(OH)_2 + CuBr_2$ and $Cu(OH)_2 + CuBr_2$ were up to 60 times the maximum theoretical, confirmed by XRD of the WFC products and scaled linearly to over 5 kW. DSC performed on FeOOH and $Cu(OH)_2 + FeBr_2$ in gold crucibles at Perkin Elmer showed up to four times the maximum theoretical energy. DSC and XRD were independently performed on the starting materials. The reaction occurred at relatively low temperature (~150 °C) compared to those of a commercial power plant (~650 °C). Since the

theoretical enthalpy of reaction is low for conventional chemistry (Table 3), it is feasible to thermally reverse the products into reactants, especially if a reactant formed in the regeneration reaction is removed. Rankine-style electrical power plants that exploit this principle were reported previously [16,17]. The results indicate that continuous generation of power liberated by forming hydrinos is commercially feasible using simplistic and efficient systems that concurrently maintain regeneration as part of the thermal energy balance. The system is closed except that only hydrogen consumed in forming hydrinos need be replaced. Hydrogen to form hydrinos can be obtained ultimately from the electrolysis of water with 200 times the energy release relative to combustion.

References
1. Mills RL. *The Grand Unified Theory of Classical Physics*; 2014 Edition. Website: http://www.blacklightpower.com/theory/bookdownload.shtml. [accessed 20.5.14]
2. Xie W, Mills RL, Good W, Makwana A, Holverstott B, Hogle N. Millsian 2.0: A molecular modeling software for structures, charge distributions and energetics of biomolecules. Phys Essays 2011;24:200–212.
3. Mills RL, Holverstott B, Good W, Makwana A. Total bond energies of exact classical solutions of molecules generated by Millsian 1.0 compared to those computed using modern 3-21G and 6-31G* basis sets. Phys Essays 2010;23:153–199; doi: 10.4006/1.3310832.
4. Mills RL. Physical solutions of the nature of the atom, photon, and their interactions to form excited and predicted hydrino states. Phys Essays 2007;20:403–460.
5. Mills RL. Exact classical quantum mechanical solution for atomic helium which pedicts conjugate parameters from a unique solution for the first time. Phys Essays 2008;21:103–141.
6. Mills RL. Exact classical quantum mechanical solutions for one- through twenty-electron atoms. Phys Essays 2005;18:321–361.
7. Mills RL. The nature of the chemical bond revisited and an alternative Maxwellian approach. Phys Essays 2004;17:342–389.
8. Mills RL. Classical quantum mechanics. Phys Essays 2003;16":433–498.
9. Mills RL. The Nature of free electrons in superfluid helium—a test of quantum mechanics and a basis to review its foundations and make a comparison to classical theory. Int J Hydrogen Energy 2001;26:1059–1096.
10. Mills RL, Yu X, Lu Y, Chu G, He J, Lotoski J. Catalyst induced hydrino transition (CIHT) electrochemical cell. Int J Energy Res (2013), DOI: 10.1002/er.3142.
11. Mills RL, Lotoski J, Kong J, Chu G, He J, Trevey. High-power-density catalyst induced hydrino transition (CIHT) electrochemical cell. 2014, submitted.

12. Mills RL, Zhao G, Akhtar K, Chang Z, He J, Hu X, et al. Thermally reversible hydrino catalyst systems as a new power source. Int J Green Energy 2011;8:429–473.

13. Mills RL, Akhtar K, Zhao G, Chang Z, He J, Hu X, et al. Commercializable power source using heterogeneous hydrino catalysts. Int J Hydrogen Energy 2010;35:395–419, doi: 10.1016/j.ijhydene.2009.10.038.

14. Mills RL, Zhao G, Akhtar K, Chang Z, He J, Lu Y, et al. Commercializable power source from forming new states of hydrogen. Int J Hydrogen Energy 2009;34:573–614.

15. Jones WJ, Stoicheff BP. Inverse Raman spectra: Induced absorption at optical frequencies, Phys Rev Lett 1964;22(13):657–659.

16. Mills RL, Nansteel M, Good W, Zhao G. Design for a BlackLight Power multi-cell thermally coupled reactor based on hydrogen catalyst systems, Int J Energy Res 2012;36:778–788, doi: 10.1002/er.1834.

17. Mills RL, Zhao G, Good W. Continuous thermal power system. Appl Energy 2011;88:789–798, doi: 10.1016/j.apenergy.2010.08.024.

18. Knacke O, Kubascheeski O, Hesselmann K. *Thermochemical Properties of Inorganic Substances*, 2nd Ed., Springer-Verlag Berlin, Heidelberg 1991.

19. Lide DR. *CRC Handbook of Chemistry and Physics*, 88th Edition, CRC Press, Taylor & Francis, Boca Raton, (2007-8).

20. Dean JA. *Lange's Handbook of Chemistry*, Fifteenth Edition, McGraw-Hill Professional, New York, (1999).